WILEY | Hindawi

Research Article

Numerical Simulation of Time-Varying Characteristics in a High-Permeability Sandstone Reservoir: A Case of Gaoqian Southern Area

Hui Xu [ID],[1] Guofeng Cheng,[2] Nannan Liu [ID],[1] Lizhi Wang,[3] Zhenghuai Guo,[1] Xiang Wang,[1] Xiangji Dou [ID],[1] Juan Li,[3] Shangping Chen,[1] and Xing Shi[1]

[1]*School of Petroleum and Natural Gas Engineering, Changzhou University, Changzhou, Jiangsu 213164, China*
[2]*Changqing Oilfield No.5 Oil Production Plant, PetroChina, Xi'an, Shanxi 710000, China*
[3]*Key Laboratory of Shallow Geothermal Energy, Ministry of Natural Resources of the People's Republic of China, Beijing 100195, China*

Correspondence should be addressed to Hui Xu; xuhui@cczu.edu.cn and Nannan Liu; 1753631088@qq.com

In the process of long-term water flooding in the Gaoqian Southern Area with an average porosity of 30% and an average permeability of $1333.5 \times 10^{-3} \, \mu m^2$, the fluid-solid interaction among oil, water, and rock has a great influence on the pore structure. It has resulted in changes in reservoir parameters with the extension of time. This paper used electron microscopy scanning, mercury injection, X-ray diffraction, physical properties, and oil-water relative permeability curves to study the variation of clay mineral content, pore throat structure, porosity, permeability, and relative permeability curves of high-permeability sandstone after high-pressure water flooding. The results showed that clay minerals such as montmorillonite and kaolinite were dissolved, hydrated, and migrated after long-term water flooding, which resulted in the decrease of clay mineral content in fine sandstone and medium sandstone, the increase of pore throat radius, and the decrease of displacement pressure, median pressure, and separation coefficient. The saturation of the isotonic point of the oil-water relative permeability curve was obviously shifted to the right, the hydrophilicity was significantly enhanced, and the porosity and permeability were effectively improved, but there was a blockage of the throat less than $2 \, \mu m$ in the fine sandstone. In addition, this paper established the equations of water injection, permeability, irreducible water saturation, residual oil saturation, and oil-water relative permeability curve coefficient and establishes the initial permeability model with the well data before water flooding. The logging interpretation results of development wells in the process of water flooding as verification data were used, and the relative error of permeability far lower than the general requirement of permeability error within an order of magnitude was less than 30%, which verified the rationality of the method.

1. Introduction

For different types of reservoirs, water flooding is widely used because of its high economic efficiency and environmental safety [1, 2]. Under natural conditions, the mineral components and fluids of the reservoir coexist in the porous medium and reach the equilibrium state under the formation conditions (REF). Water flooding is the most widely used method of improving the ultimate oil recovery (IOR) including artificial water flooding and natural water flooding

[3–9]. However, in the process of water flooding development, the decrease of reservoir temperature and pressure and the change of fluid properties lead to the break of the equilibrium, which affects the development of the oilfield [10]. The erosion of injected water causes physical changes in reservoir structure, and the incompatibility between injected water properties and reservoirs causes chemical effects such as water swelling, crystallization, precipitation, and dissolution of special minerals in reservoirs [11]. These two effects ultimately lead to the following: (1) reservoir

damage—this is mainly because the formation water and reservoir incompatibility also led to reservoir damage and plug pore throats, which is attributed to sensitive mineral hydration expansion, dispersion, and migration [12]—and (2) the formation of dominant channels—this is mainly because the dissolution and migration of minerals in porous media lead to pore growth and throat evolution, thus spontaneously forming dominant channels, so the fluid flow capacity in the formation has been significantly improved in some areas [13]. With the development of water injection, the reservoir heterogeneity is getting stronger and stronger, which seriously affects water flooding development [14].

Many scholars have studied the reservoir after water flooding and found that the long-term fluid-solid interaction between oil, water, and rock has a great influence on the pore structure. After long-term water flooding, reservoir parameters such as porosity, permeability, wettability, and relative permeability will change [15–24]; this change in reservoir properties becomes more pronounced over time, ultimately affecting oil recovery.

In order to study the change of parameters with time after water flooding, the researchers had predicted by establishing numerical model and fitting relationship. A dynamic network model was used to study the effect of the displacement rate on the relative imbibition permeability and the residual saturation. Loahardjo et al. [19] proved through experiments that the amount of remaining oil decreased significantly during continuous water injection and the relative permeability curve changed with the amount of water injected. A numerical simulation method was proposed to simulate the variation of relative permeability with time [24]. The method was studied for determining the relative permeability of the inverted five-spot well pattern over time by numerical simulation [10]. The erosion intensity by displacement flux was characterized [25]. They obtained two relative permeability curves through high-intensity water flooding experiments and established a two-dimensional five-point model. Finally, the method was verified by an actual reservoir in a mature oilfield. For different water flooding reservoirs, the injection-production rate is quite different. The change of reservoir parameters is affected by cumulative injection-production [26–28]. Therefore, it is not accurate to use time variable to characterize the variation of relative permeability.

This paper uses the method of combining coring well reservoir test and displacement experiment to study the time-varying problem of water flooding reservoir with high-permeability sandstone in Gaoqian Southern Area as the research object. The mechanism of reservoir blockage or formation of dominant channel is analyzed, and the time-varying law of reservoir during long-term water flooding development is revealed. Finally, based on the data of core displacement experiment, this paper constructs the mathematical equations of water injection and permeability increase, irreducible water saturation, residual oil saturation, and oil-water relative permeability curve coefficient and establishes the initial permeability model with the well data before water flooding. The logging interpretation results of development wells in the process of water flooding are veri-fied. The results show that this method can reasonably predict the change of permeability. The conclusion of this paper has important application value for guiding long-term water injection to enhance oil recovery.

2. Samples and Methods

The lithology of the reservoir in the Gaoqian Southern Area is mainly medium-fine sandstone and has transitional type, and a small part is unequal-grained sandstone. The sandstone maturity is low and the sorting is poor. The statistics of rock mineral composition in Gao 104-5 block are shown in Table 1. The quartz content is 33~86%, average 45.1%; feldspar content 8~52%, average 25.3%; and cutting content 6~45%, average 28%; the interstitial materials are mainly mud, with the content of 3~41% and the average of 20.8%. Carbonate minerals are very few. The cementation type is mainly pore cementation. The debris particles are subangular to subcircular, and the sorting is medium.

The absolute content of clay minerals is 10.2% in the reservoir of Gao 104-5 area. After X-ray diffraction analysis of clay minerals, the content of clay minerals in well GJ514-5 is shown in Table 2, and the composition is mainly montmorillonite accounting for 50.1% and kaolinite accounting for 28.5%. In addition, as shown in Table 3, according to the statistics of core physical analysis data, the porosity ranges from 22.5% to 35.8%, with an average of 30%; the permeability range is $51.4 \sim 5328 \times 10^{-3} \, \mu m^2$, with an average of $1333.5 \times 10^{-3} \, \mu m^2$.

As shown in Figure 1, the reservoir space types of the reservoir in this block are primary intergranular pores, intergranular dissolved pores, a small number of microfractures, intragranular dissolved pores, and mold pores. The average pore throat radius varies greatly, ranging from 0.2 to $16.3 \, \mu m$, with an average of $5.5 \, \mu m$. The main flow pore throat radius varies from 0.1 to $63 \, \mu m$, with an average of $10.0 \, \mu m$, and the relative sorting coefficient is 0.1 to 7.4, with an average of 3.3. Oil displacement pressure is small, an average of 0.19 MPa. The mercury saturation is large, with an average of 79.4%, belonging to the range of middle-large pore throat.

3. Results and Discussion

Long-term water flooding will lead to significant changes in reservoir pore structure, and the change in pore structure is directly related to the composition, occurrence, and content of clay minerals in pores. Mechanical transport and hydration are the main reasons for the decrease in clay mineral content and the heterogeneous change of pore structure.

3.1. Reservoir Characteristic Variation after Water Flooding

3.1.1. Changes in Clay Minerals during Water Flooding. Comparing the analysis and test results of different lithofacies original rock samples and water flooding 60PV in coring wells, it is found that the clay mineral content of fine sandstone facies and medium sandstone facies decreases

TABLE 1: Rock mineral composition in the Gao 104-5 area.

Thin layer	Well section (m)	Quartz		Feldspar		Debris		Fillings	
		Scope	Mean/block	Scope	Mean/block	Scope	Mean/block	Scope	Mean/block
12	1853.00~1892.36	35~86	53.7/9	8~39.5	25.2/9	6~33	19.8/9	11~41	24.9/9
132	1863.16~1906.96	33~60	42.1/41	10~52.1	25.2/41	9.7~45	31.5/41	12~40	21.6/41
133	1890.91~1922.47	40~61	49.3/11	10~32.9	25.9/11	8.6~37	21.9/11	3~26	14.5/11
Average	1853.00~1922.47	33~86	45.1/61	8~52.1	25.3/61	6~45	28.0/61	3~41	20.8/61

TABLE 2: Clay mineral contents in well GJ514-5.

Thin layer	Well section (m)	Number of blocks	Absolute content of clay minerals (%)		Relative content of clay minerals (%)						
			Scope	Mean value	S	I/S	I	K	C	R	%S
12	1853.00~1892.21	7	3.9~30	17.6	55.3		11.0	23.9	9.9	Ro	70.0
13^2	1869.20~1892.21	37	1.6~46	8.1	42.9		9.6	31.1	13.8	Ro	78.6
13^3	1890.10~1922.12	11	7~26.4	12.6	67.0	30.5	7.5	25.5	6.5	Ro	60.0
Average	1853.00~1922.12	55	1.6~46	10.2	49.3	30.5	9.4	29.1	11.8	Ro	73.8

S: montmorillonite; I/S: illite-smectite mixed layers; K: kaolinite; I: illite; C: chlorite; R: degree of order; Ro: disorder; %S: mixed layer ratio.

TABLE 3: Porosity and permeability results in the Gaoqian Southern Area.

Thin layer	Well section (m)	Porosity (%)		Permeability ($10^{-3}\ \mu m^2$)	
		Scope	Mean/number	Scope	Mean/number
8	1800.37~1862.4	26.8~35.3	30.5/52	171~3901	1533.3/47
9	1880.94~1886.85	28.1~28.4	28.3/2	470~1123	796.5/2
12	1855.18~1904.15	22.7~30.3	26.6/7	51.4~1900	565.6/7
132	1870.36~1881.5	22.5~35.14	32.2/52	55.1~5328	1342.3/50
133	1895.35~1898.76	26.0~33.8	30.4/13	76.5~2678	1146.7/9
Average			30.0/125		1333.5/117

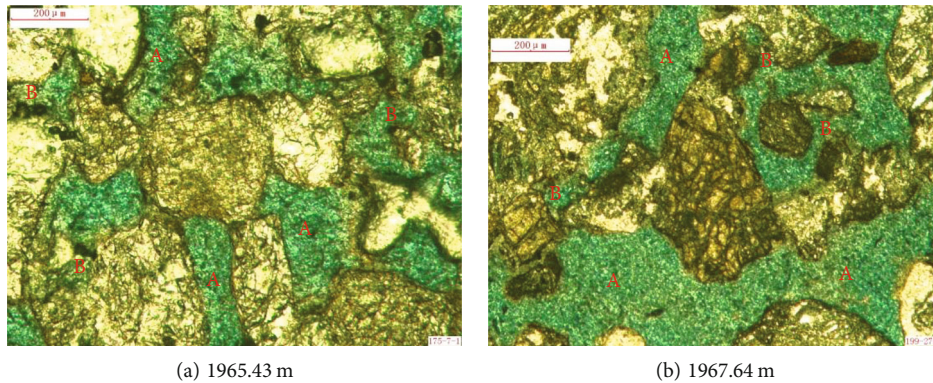

(a) 1965.43 m   (b) 1967.64 m

FIGURE 1: Images of different depths of well GJ514-5 casting sheet (A—primary intergranular dissolved pore, B—intergranular dissolved pore).

after water flooding, and the change rate of clay content of fine sandstone is generally large, as shown in Table 4.

In the fine sandstone facies, the average pore throat radius is small, and the reservoir clay mineral content is relatively high. In addition to the development of more montmorillonite and illite mixed layer in Figure 2(a)), there are more kaolinite and other clay minerals. After long-term water flooding, on the one hand, these clay minerals are dispersed and mechanically transported due to loose structure and poor adhesion, resulting in local throat widening and small seepage resistance, forming dominant seepage channels. On the other hand, the water-sensitive minerals such

TABLE 4: Changes of clay mineral contents before and after water flooding.

Lithofacies	Displacement stage	Overall amount (%)	Rate of change	S (%)	Rate of change	I/S	Rate of change	I (%)	Rate of change	K (%)	Rate of change	C (%)	Rate of change
Fine sandstone facies	Before water flooding	20.0	-43.3	6.8	-47.0	6.2	-37.1	1.2	-62.0	4.4	-29.0	1.4	-82.5
	After water flooding	11.3		3.6		3.9		0.5		3.1		0.2	
Middle sandstone facies	Before water flooding	14.6	-31.8	7.2	-21.1	0.0	/	1.5	-88.4	4.7	-42.5	1.2	15.0
	After water flooding	10.0		5.7		0.0		0.2		2.7		1.4	

S: smectite; I: illite; K: kaolinite; C: clay.

(a) Montmorillonite in fine sandstone facies (2.5PV)

(b) Montmorillonite in fine sandstone facies (60PV)

(c) Kaolinite in fine sandstone facies (2.5PV)

(d) Kaolinite in fine sandstone facies (60PV)

(e) Montmorillonite in middle sandstone facies (2.5PV)

(f) Montmorillonite in middle sandstone facies (60PV)

(g) Kaolinite in middle sandstone facies (2.5PV)

(h) Kaolinite in middle sandstone facies (60PV)

FIGURE 2: The change of clay mineral content and morphology under different water flooding PV.

as montmorillonite will destroy, collapse or even dissolute due to hydration, which will be washed away by water, further widen the seepage channels as shown in Figures 2(b) and 2(c). At the same time, in the local small pore throat, clay minerals plug the pore throat as shown in Figure 2(d).

In the middle sandstone facies, the clay mineral content is relatively low, and a small amount of montmorillonite is displaced due to long-term contact with the injected water in Figures 2(e) and 2(f)), and kaolinite is rapidly displaced by erosion in Figures 2(g) and 2(h). Compared with the fine sandstone reservoir, due to the development of medium and large pore throats before water flooding, the decrease of clay minerals after water flooding is small, and the degree of heterogeneity is relatively small.

3.1.2. Changes in Pore Structure. The pore space of fine sandstone facies is mostly occupied by clay minerals before water flooding as shown in Figure 3(a), which is dominated by mesopores and fine throats. The distribution of pore throat radius is unimodal. After long-term mining, the unimodal distribution tends to disperse, and clay minerals are locally enriched. The pore throats less than $5 \mu m$ and greater than $25 \mu m$ increase significantly in Figure 4(a), forming medium-coarse pore throats, and local pore throats less than $2 \mu m$ are blocked in Figures 3(b) and 3(c)), forming fine pore throats and enhancing heterogeneity.

Before water flooding, the heterogeneity of pore structure in the middle sandstone facies is strong, local clay minerals are enriched, mainly in the middle pore and middle

(a) Before water flooding, P35, 2046 m　　(b) 2.5PV, P35, 2046 m　　(c) 60PV, P35, 2046 m
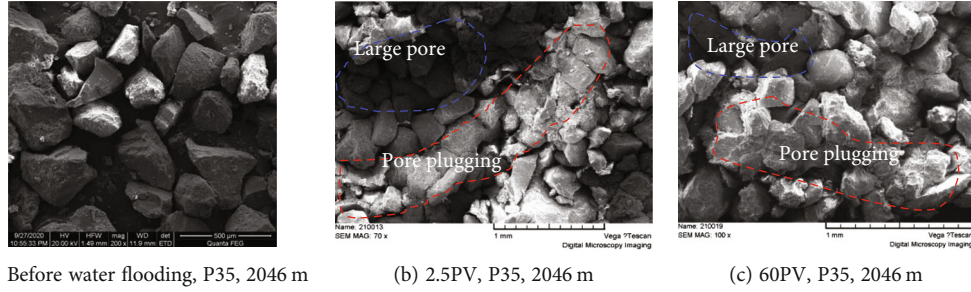
FIGURE 3: Heterogeneous characteristics of microscopic pore structure of fine sandstone facies reservoir before and after water flooding in well 16-1.
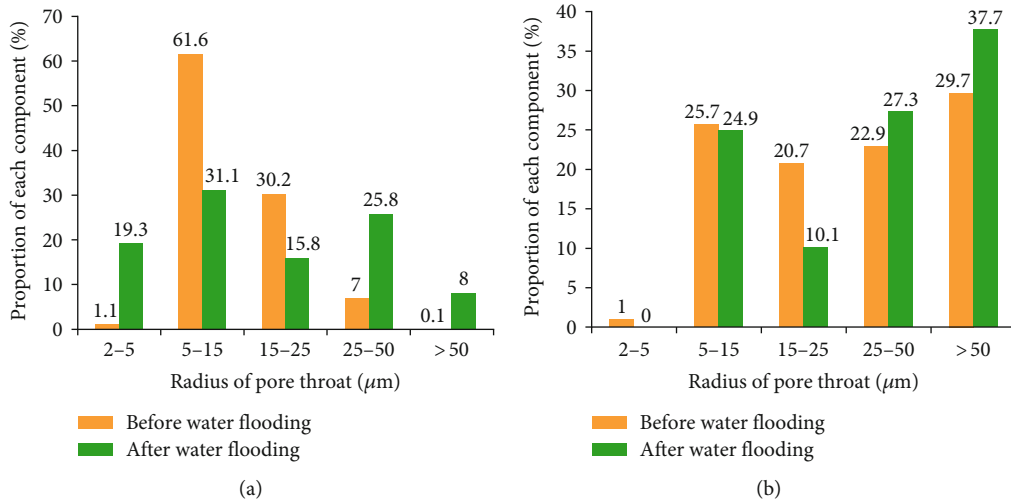

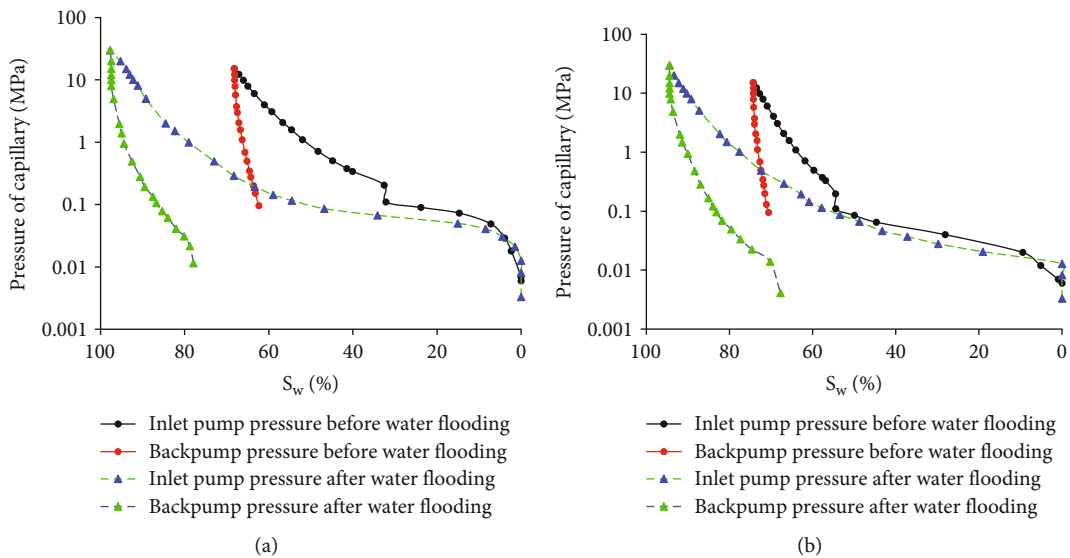FIGURE 4: Comparison of pore throat radius before and after different lithofacies water flooding.

FIGURE 5: Comparison of capillary pressure curves before and after water flooding in different lithofacies.

throat, and the distribution range of pore throat radius is large, showing a double peak shape. After long-term mining, clay minerals are washed out, and the pore throat radius is double peak offset. The pore throat larger than $50\,\mu m$ is

increased, followed by 25-50 μm, and the reservoir physical properties are significantly improved in Figure 4(b).

As shown in Figure 5, by comparing the capillary pressure curves before and after water flooding in different
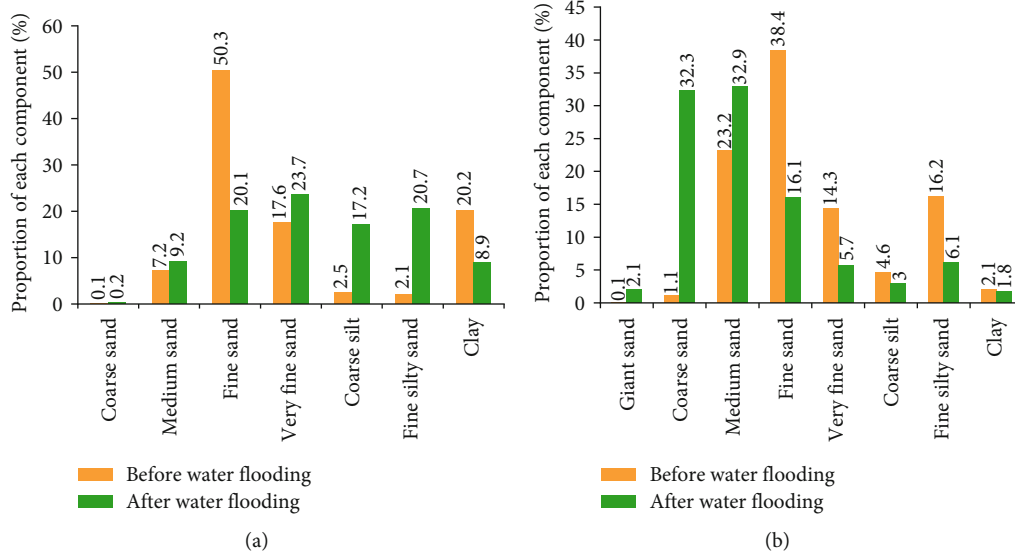
FIGURE 6: Comparison of particle size before and after water flooding in different lithofacies.
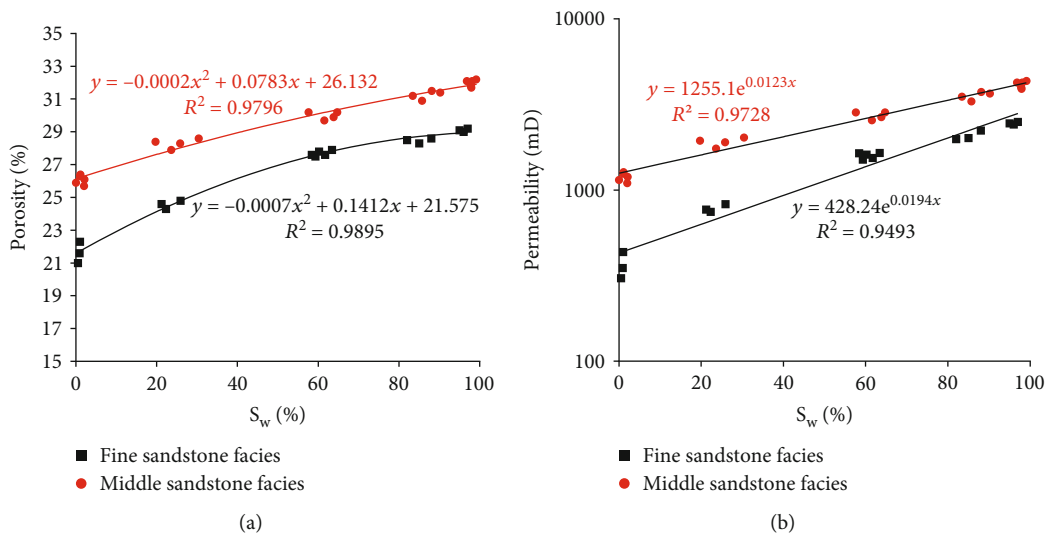

FIGURE 7: Changes of physical properties of different lithofacies reservoirs during water flooding.

TABLE 5: Changes in porosity and permeability before and after water flooding.

Lithofacies	Free period		Extra high water cut stage		Multiple	
	Por (%)	Perm (mD)	Por (%)	Perm (mD)	Por	Perm
Fine sandstone facies	21.6	363	29.4	2453	1.36	6.8
Middle sandstone facies	26.1	1189	32	4140	1.23	3.5

TABLE 6: Changes of reservoir wettability before and after water flooding.

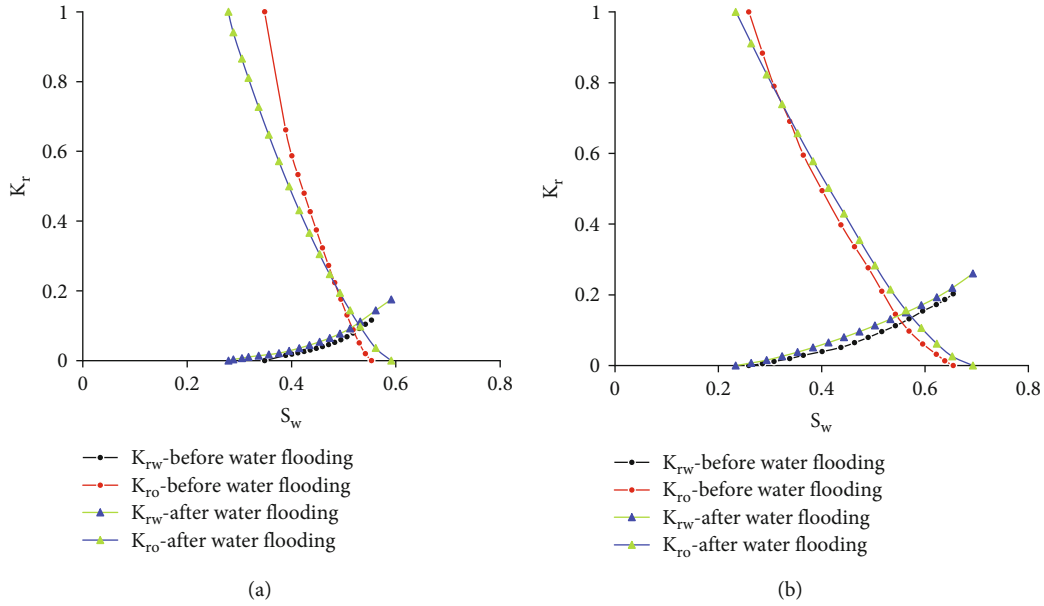| Lithofacies	Wettability before water flooding (wetting angle)	Wettability after water flooding (wetting angle)
Fine sandstone facies	Neutral (90°)	Strong hydrophilic (51°)
Middle sandstone facies	Neutral-weakly hydrophilic (82°)	Strong hydrophilic (43°)

(a)

(b)

FIGURE 8: Comparison of relative permeability curves before and after water flooding in different lithofacies.

TABLE 7: Results of core water flooding experiment.

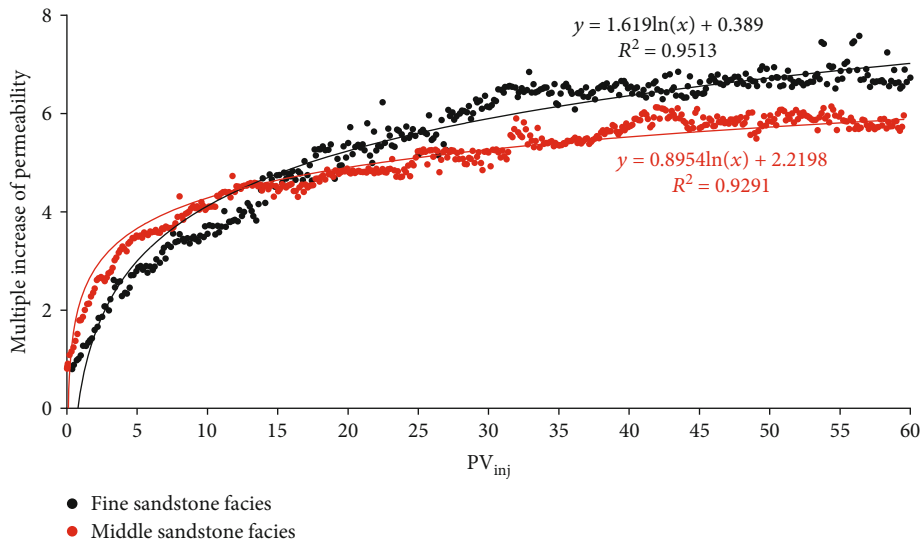| Well number	Depth (m)	Lithofacies	PV_{inj}	Initial permeability (mD)	Final permeability (mD)
16-1	2041	Fine sandstone facies	60	379	2548.775
16-1	2048	Middle sandstone facies	60	1034	6152.3

FIGURE 9: The relationship between the permeability increase multiple of different lithofacies and injected PV in Gao 104-5 block.

lithofacies reservoirs, it is found that the displacement pressure decreases after water flooding in different lithofacies reservoirs, the skewness increases significantly, the mercury injection and mercury withdrawal curves slow down, the median pressure and sorting coefficient decrease, and the average pore throat radius increases, indicating that the reservoir connectivity is enhanced and the pore structure is improved after water flooding. Among them, the parameters of fine sandstone facies reservoir change the most, the reservoir changes greatly, and the improvement effect is obvious.

3.2. Changes in Granularity. Due to the common sand production phenomenon in the process of water flooding development, the change of reservoir particle size before and after
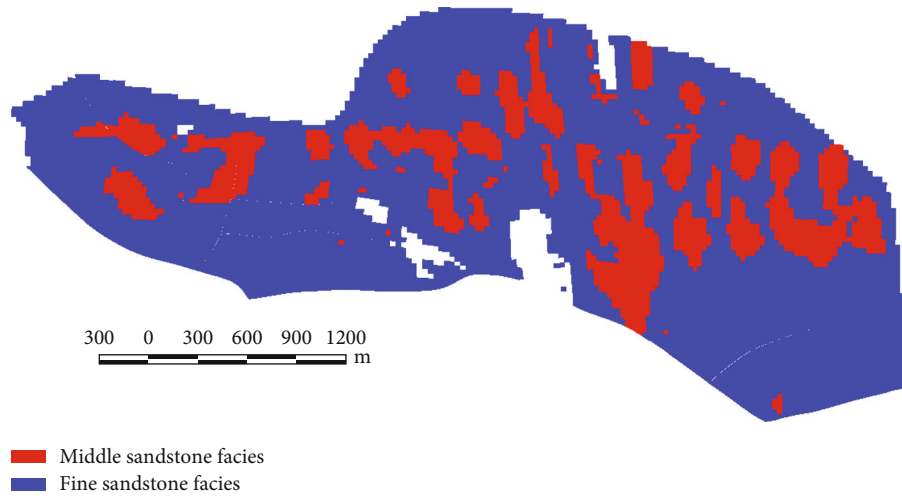
Middle sandstone facies
Fine sandstone facies

FIGURE 10: Lithologic model of $Ng_{13}{}^3$ sublayer.

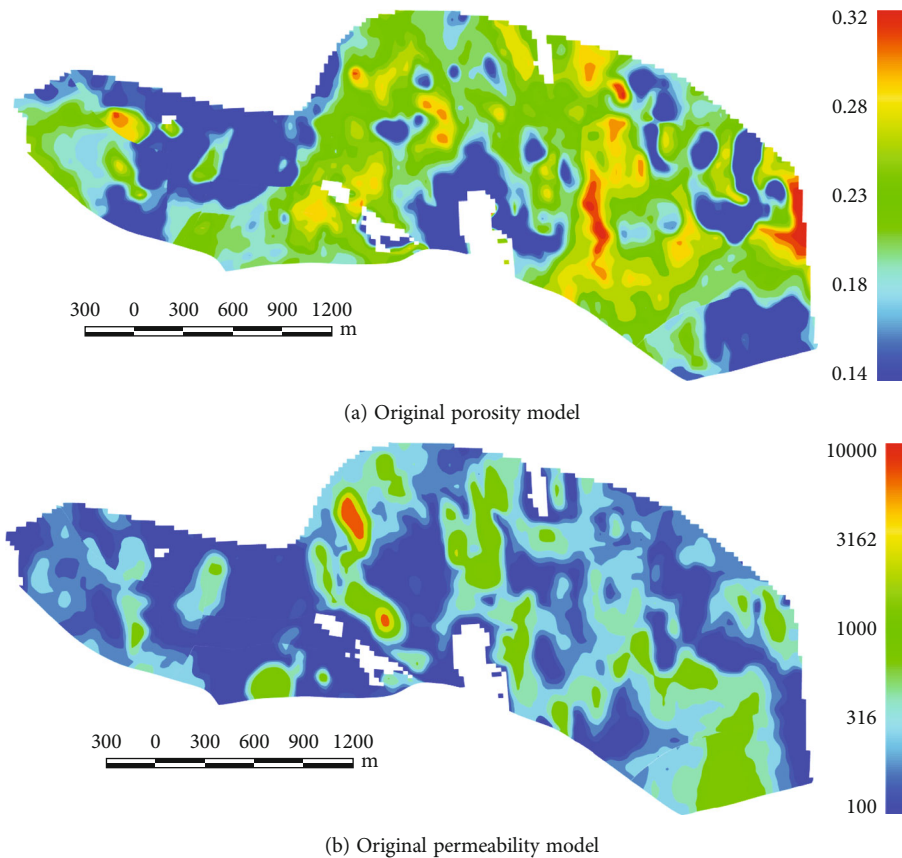(a) Original porosity model

(b) Original permeability model

FIGURE 11: Original geological model of $Ng_{13}{}^3$ sublayer.

water flooding is analyzed. As shown in Figure 6, it is considered that the proportion of fine-grained components decreases as a whole after water flooding. The fine sandstone reservoir is dominated by fine sand and clay particles before water flooding, showing bimodal characteristics. After long-term development, the particle size distribution tends to be dispersed, the fine sand and clay particles are significantly reduced, and the proportion of other components is increased. The reason is the dissolution and hydration of clay minerals and the migration of fine sand particles. Due to pore blockage, the proportion of coarse silt and fine silt increased greatly. Before water flooding, the middle sandstone facies reservoirs are dominated by middle sand and fine sand particles and also show bimodal characteristics. After long-term development, the particle size distribution changes from bimodal to unimodal, and the main peak shifts to the middle

TABLE 8: Statistics of oil-water relative permeability curve parameters under different water injection multiples.

| PV_inj | Fine sandstone facies | | | | | | | Middle sandstone facies | | | | | |
|--------|--------|--------|-----------|-----------|-----------|-----------|--------|--------|-----------|-----------|-----------|-----------|
| | S_{wi} | S_{or} | $a - K_{ro}$ | $b - K_{ro}$ | $a - K_{rw}$ | $b - K_{rw}$ | S_{wi} | S_{or} | $a - K_{ro}$ | $b - K_{ro}$ | $a - K_{rw}$ | $b - K_{rw}$ |
| 0.01 | 0.348 | 0.447 | 429.33 | -18.19 | 0.0001 | 12.411 | 0.259 | 0.365 | 17.938 | -10.618 | 0.001 | 8.702 |
| 2.5 | 0.316 | 0.416 | 117.61 | -14.94 | 0.0002 | 11.635 | 0.241 | 0.345 | 12.651 | -9.756 | 0.0016 | 7.954 |
| 10 | 0.285 | 0.397 | 53.14 | -13.05 | 0.0003 | 10.942 | 0.232 | 0.328 | 8.864 | -8.546 | 0.0025 | 7.377 |
| 60 | 0.264 | 0.384 | 39.72 | -12.06 | 0.00045 | 10.286 | 0.216 | 0.319 | 7.064 | -7.925 | 0.0031 | 7.073 |

(a)

(b)
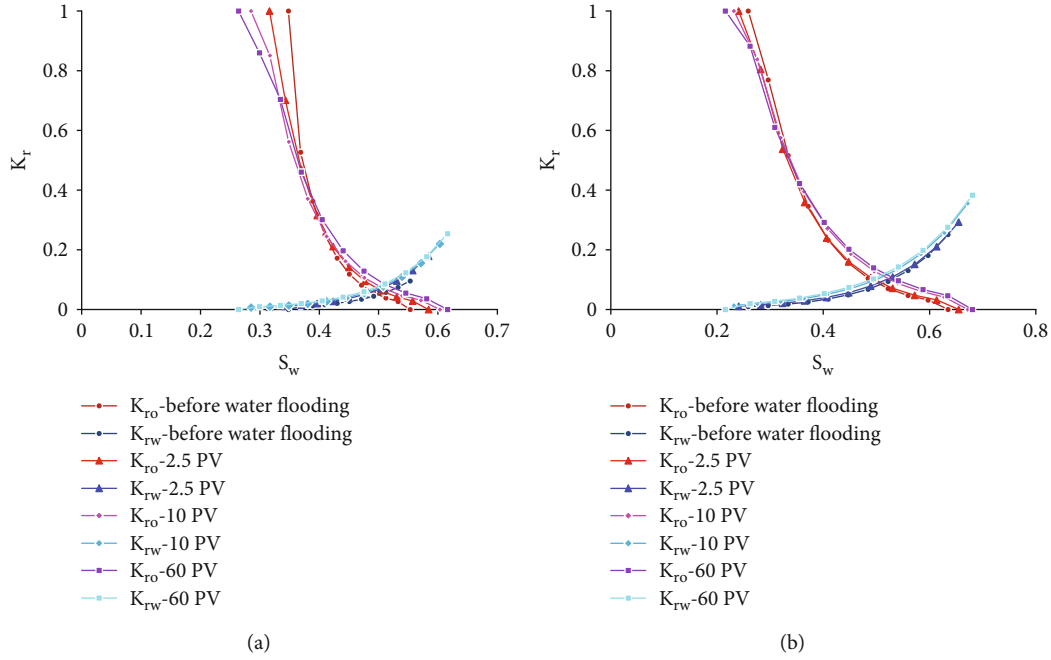
FIGURE 12: Relative permeability curves of different lithofacies after different water injection multiples.

coarse sand component, indicating that the fine grain composition moves with water.

3.3. Changes in Reservoir's Physical Properties. Considering that the reservoir physical properties will change after water flooding, this paper selects the core test data and production data of wells with production above $60 \, \text{m}^3/\text{d}$ for comparative analysis. It can be seen from Figure 7 that the porosity and permeability increase significantly in different water-bearing stages, which indicates that the long-term water injection scouring makes the reservoir physical properties improve obviously.

However, the degree of transformation of different lithofacies reservoirs by long-term erosion affecting the improvement of the seepage capacity of fine sandstone facies reservoirs is the best. As shown in Table 5, the porosity of fine sandstone increases by 1.36 times and the permeability increases by 6.8 times. The improvement of middle sandstone facies is relatively low, the porosity increases by 1.23 times, and the permeability increases by 3.5 times. The statistical results in Table 5 are the average values of the sample data in Figure 7. The data before water flooding is the average value of sample of water cut below 2%, while the data after water flooding is the average value of sample of water cut above 96%.

3.4. Change of Seepage Characteristics. The changes in reservoir wettability before and after water flooding are shown in Table 6. The hydrophilicity of different lithofacies reservoirs is enhanced. At the same time, according to the comparison of the relative permeability curves of different lithofacies before and after water flooding in Figure 8, it is found that the saturation of the isotonic point of different lithofacies reservoirs after water flooding is shifted to the right, which also confirms that the hydrophilicity is significantly enhanced, and the relative permeability corresponding to the isotonic point is increased, reflecting the improvement of oil-water seepage capacity.

The reasons for the strong hydrophilicity of different lithofacies in the reservoir after water flooding are mainly due to two aspects. On the one hand, the wettability of the reservoir is affected by the type of mineral components. For example, minerals such as quartz and feldspar are hydrophilic. During the long-term mining process, the surface of the particles will gradually be occupied by water, forming a water film, which enhances the hydrophilicity of the
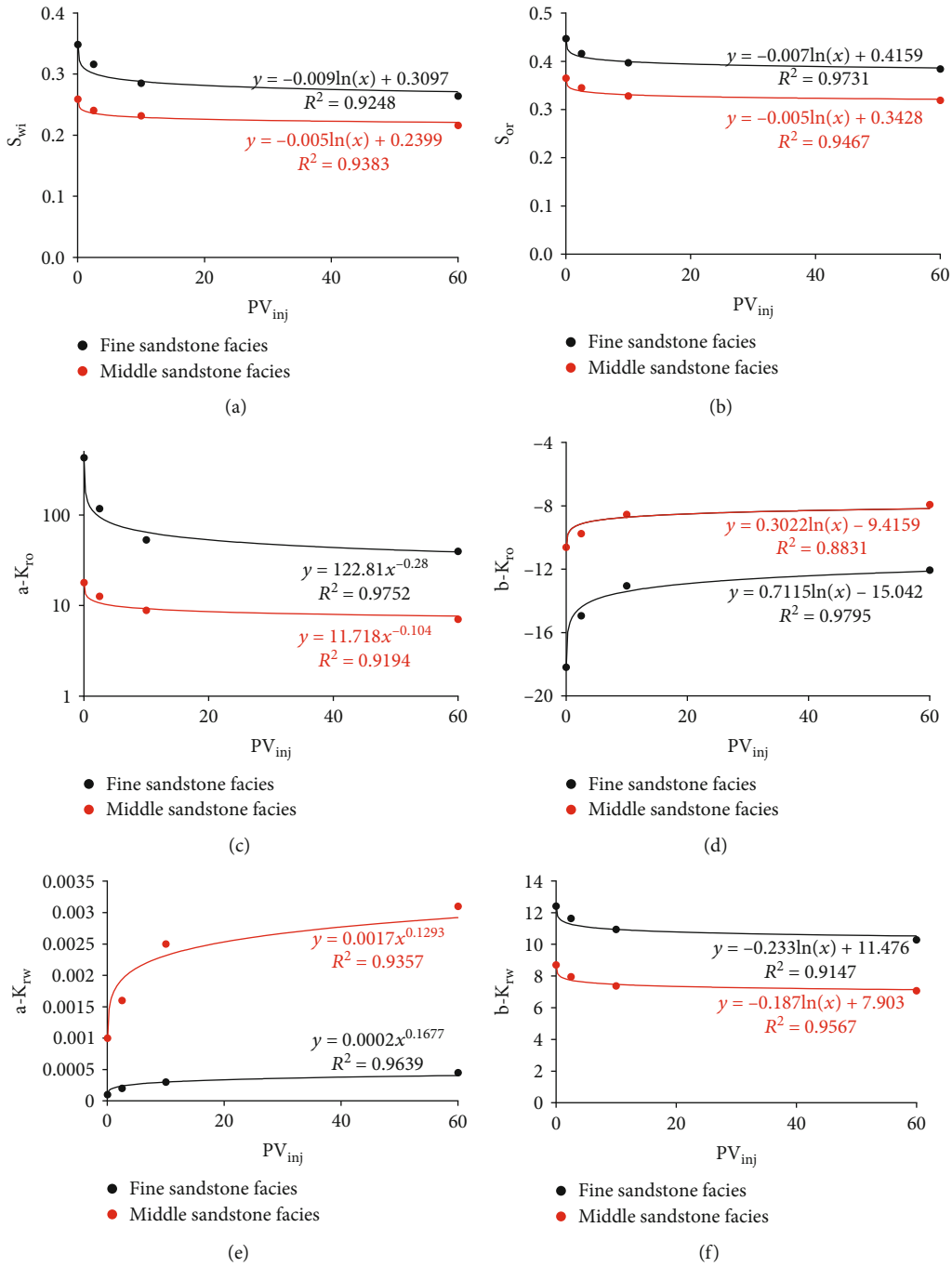
FIGURE 13: Relationship between parameters and PV_{inj}.

reservoir. On the other hand, clay minerals such as kaolinite and chlorite will increase the lipophilic properties of the reservoir. However, during the long-term scouring process, clay minerals such as kaolinite and chlorite are washed away in large quantities and moved away from the particle surface or pores, which also increases the hydrophilicity of the reservoir. At the same time, the fluid is in long-term contact with the mineral particles during the development process. After a large amount of scouring, the particle surface will become smoother, which also increases the seepage capacity of the water phase and changes to the hydrophilic direction.

3.5. Simulation Results. In this paper, considering the convergence of material balance equation and mathematical model, the change of porosity caused by the change of pore throat radius is not considered in numerical simulation engineering, and only the time-varying characteristics of permeability and oil-water relative permeability are taken as the research object.

3.5.1. Characterization of Permeability Increase Multiple. Because the reservoir physical properties of different lithofacies vary greatly, the correlation between different lithofacies
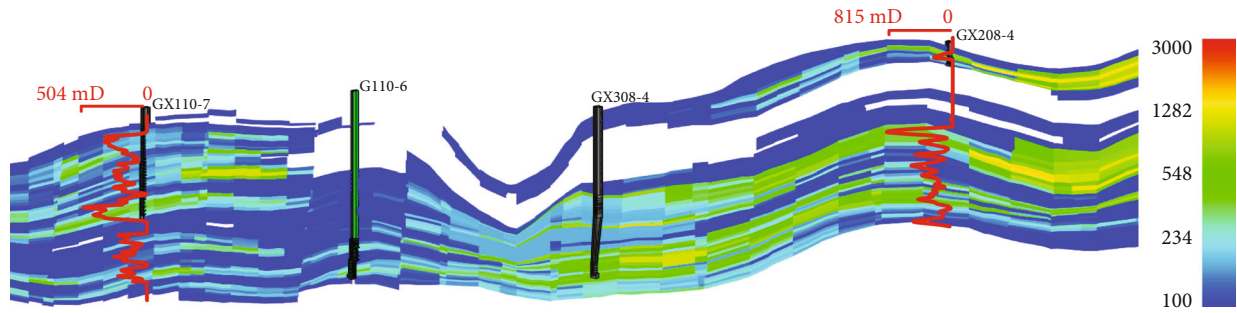
(a) Permeability cross-section of well G115-7~G119-6 (8 years)
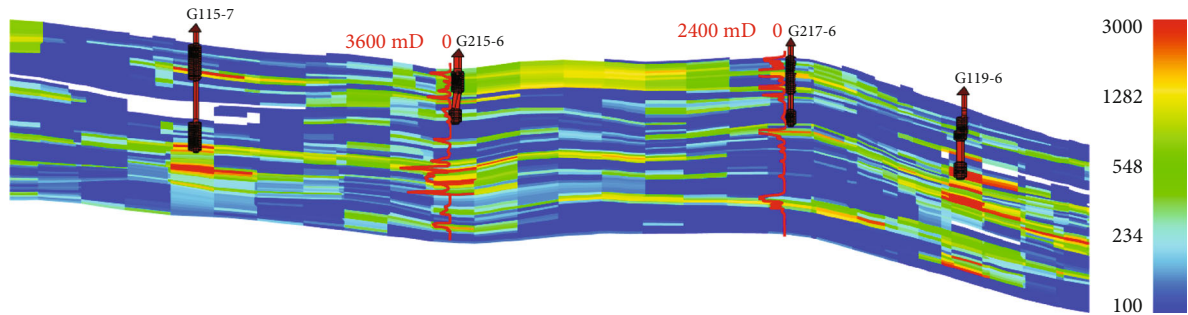
(b) Permeability cross-section of well GX110-7~GX208-4 (18 years)

Figure 14: Results of permeability prediction.

Table 9: Comparison of actual and simulated permeability of typical wells.

Times Well number		8 years		18 years	
		G215-6	G217-6	GX110-7	GX208-4
$Ng_{12}a$	Actual permeability	319	419	15	0.1
	Simulated permeability	400	323	18	0.1
$Ng_{12}b$	Actual permeability	217	775	263	178
	Simulated permeability	379	429	320	190
Ng_{13}-1a	Actual permeability	457	190	161	0.1
	Simulated permeability	374	156	267	0.1
Ng_{13}-1b	Actual permeability	125	40	198	0.1
	Simulated permeability	179	26	240	0.1
Ng_{13}-2a	Actual permeability	185	641	244	0.1
	Simulated permeability	172	473	361	0.1
Ng_{13}-2b	Actual permeability	1100	73	25	320
	Simulated permeability	840	64	29	350
Ng_{13}-2c	Actual permeability	931	51	142	270
	Simulated permeability	720	50	180	115
Ng_{13}-3a	Actual permeability	157	327	130	228
	Simulated permeability	114	279	173	256
Ng_{13}-3b	Actual permeability	293	108	25	230
	Simulated permeability	236	100	30	120
Average relative error (%)		23	18	29	26.2

(a) Profile of permeability distribution of the original model

(b) Profile of permeability distribution after water flooding (20 years)

(c) Permeability distribution of Ng_{13}^{3} sublayer (20 years)
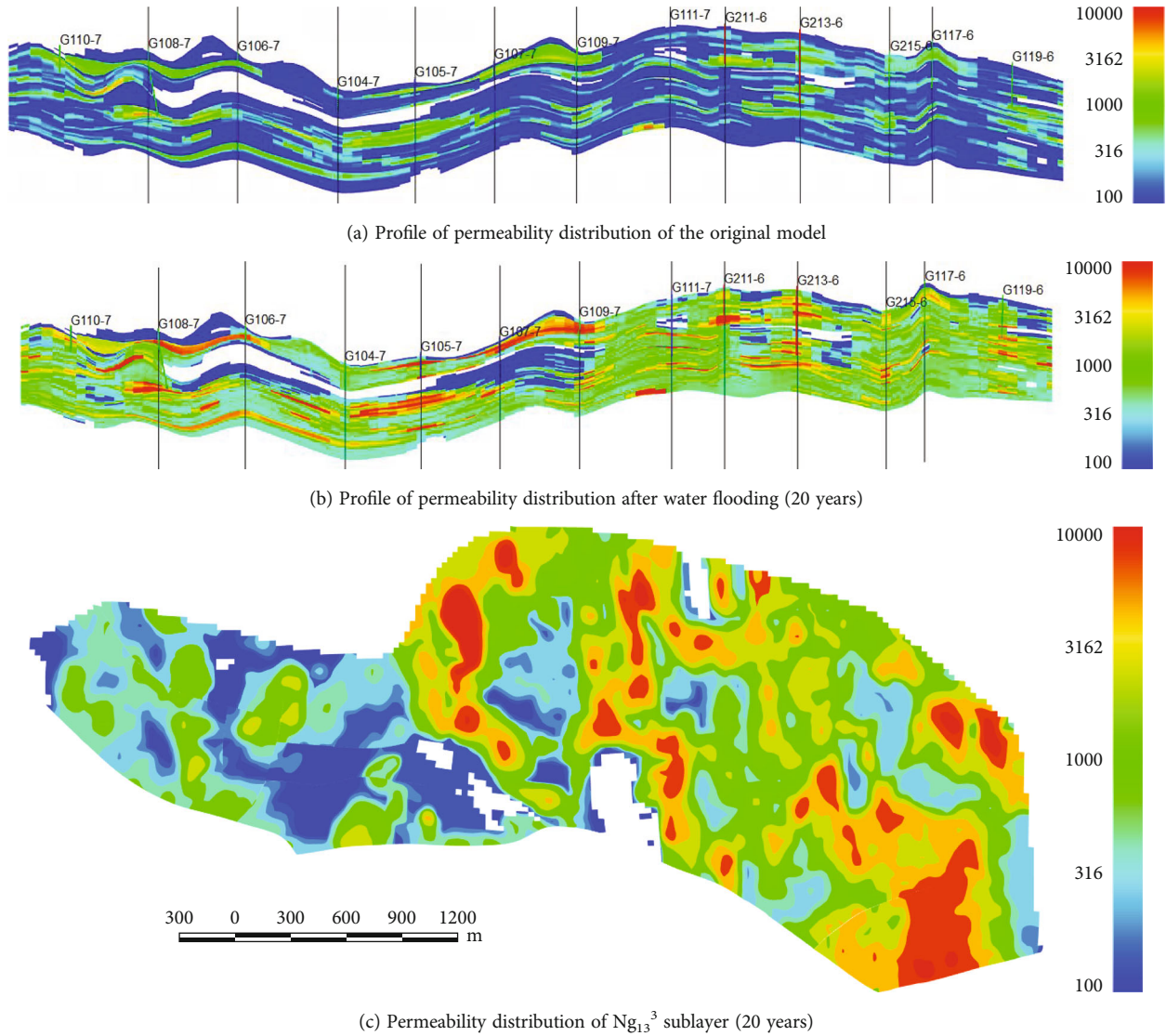
FIGURE 15: Model of permeability.

permeability in Table 7 obtained from core displacement experiment and water injection multiple is used for time-varying simulation in this paper. The simulation results are shown in Figure 9.

PV_{inj} is the ratio of the total water volume through a core to the core pore volume, and the following equation is shown.

$$PV_{inj} = \frac{Q_w}{V\varnothing_c} = \frac{Q_w}{Sl\varnothing_c}. \tag{1}$$

In this equation, PV_{inj} is the water injection multiple, Q_w is the total water volume through the core (m^3), V is the apparent volume of the core (m^3), S is the core cross-sectional area (m^2), l is the core length (m), and $\varnothing_c$ is the core porosity.

If in numerical simulation, PV_{inj} is the cumulative water injection multiple of the grid, Q_w is the total water volume

through the core (m^3), V is the volume of the grid (m^3), and $\varnothing_c$ is the porosity of the grid.

In this paper, the Petrel software is used to establish the fine and medium sandstone lithology model; the numerical model is shown in Figure 10. In the process of numerical simulation, each grid calls the relationship function between cumulative water injection multiple and permeability increase multiple according to the corresponding lithology to calculate the instantaneous permeability of the grid.

Then, this paper uses the wells before water injection to establish the original geological model and uses the well data after water injection as the verification well. The original porosity model is shown in Figure 11.

3.5.2. Curve Characterization of Oil-Water Relative Permeability. In this paper, core samples were used for water flooding experiments to measure the oil-water relative permeability parameters of fine sandstone and middle sandstone cores after
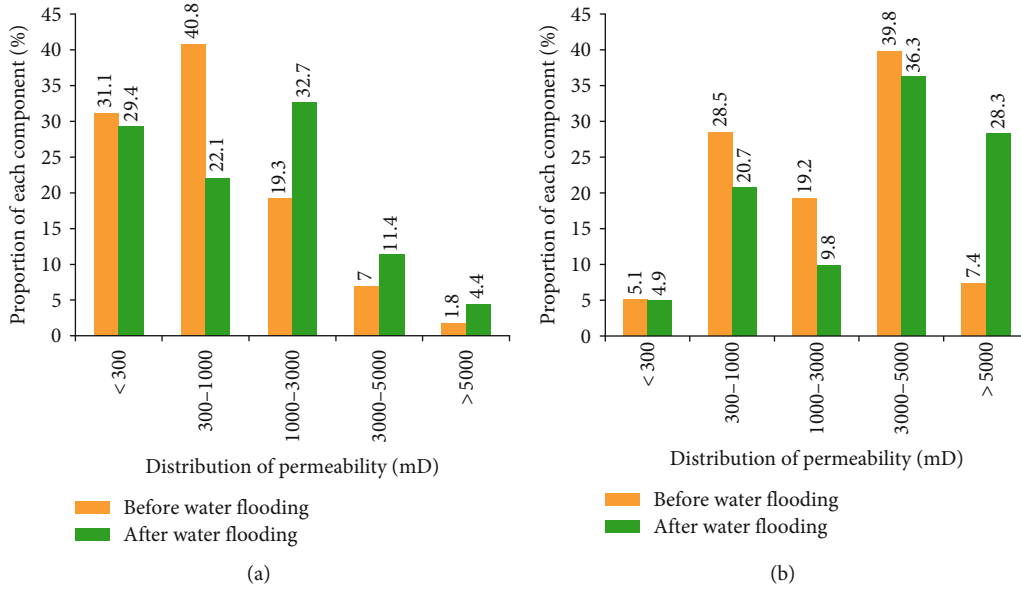
FIGURE 16: Statistics of permeability distribution range after water flooding in different lithofacies (20 years).
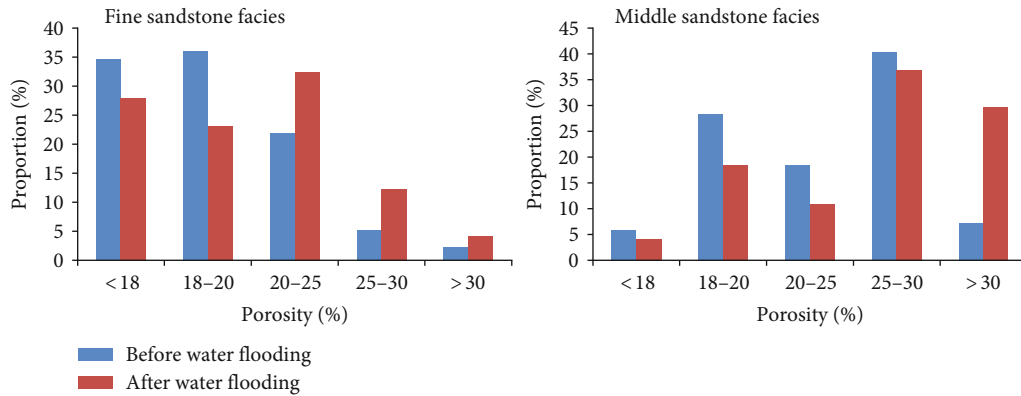

FIGURE 17: Statistics of porosity distribution range after water flooding in different lithofacies (20 years).

different water injection. The results of the measurement parameters are shown in Table 8.

Then, this paper uses the parameters to draw the relative permeability curves of different lithofacies after different water injections. As shown in Figure 12, it can be seen that the irreducible water saturation and residual oil saturation of the two sandstones gradually decrease with the increase of PV_{inj}.

The coefficients a and b in the relationship between oil and water relative permeability curves and water saturation also show a very good fit with PV_{inj}, as shown in Figure 13.

$$K_r = a \bullet e^{b \bullet S_w}. \qquad (2)$$

In each time step of the calculation process, the cumulative water injection of each grid is counted. According to the fitting formula of the following diagram, the S_{wi}, S_{or}, a, and b are calculated, respectively, to obtain the oil-water relative permeability curve of the grid.

S_{wi} is the irreducible water saturation; S_{or} is the residual oil saturation; $a - K_{ro}$ is the oil relative permeability coefficient a; $b - K_{ro}$ is the oil relative permeability coefficient b; $a - K_{rw}$ is the water relative permeability coefficient a; $b - K_{rw}$ is the water relative permeability coefficient b.

4. Verification of Numerical Simulation Results

4.1. Verification of Permeability Prediction Results. Using the above method for permeability time-varying, the prediction results are shown in Figure 14. As shown in Table 9, the logging interpretation results of two new wells after 8 years of water injection are compared with the predicted permeability results at the well point. The permeability values are relatively close, and the average relative error is only 18%~23%. For the two new wells after 18 years of water injection, the average relative error between the logging interpretation results and the predicted permeability results is only 26.2~29%. Considering that the error range of permeability
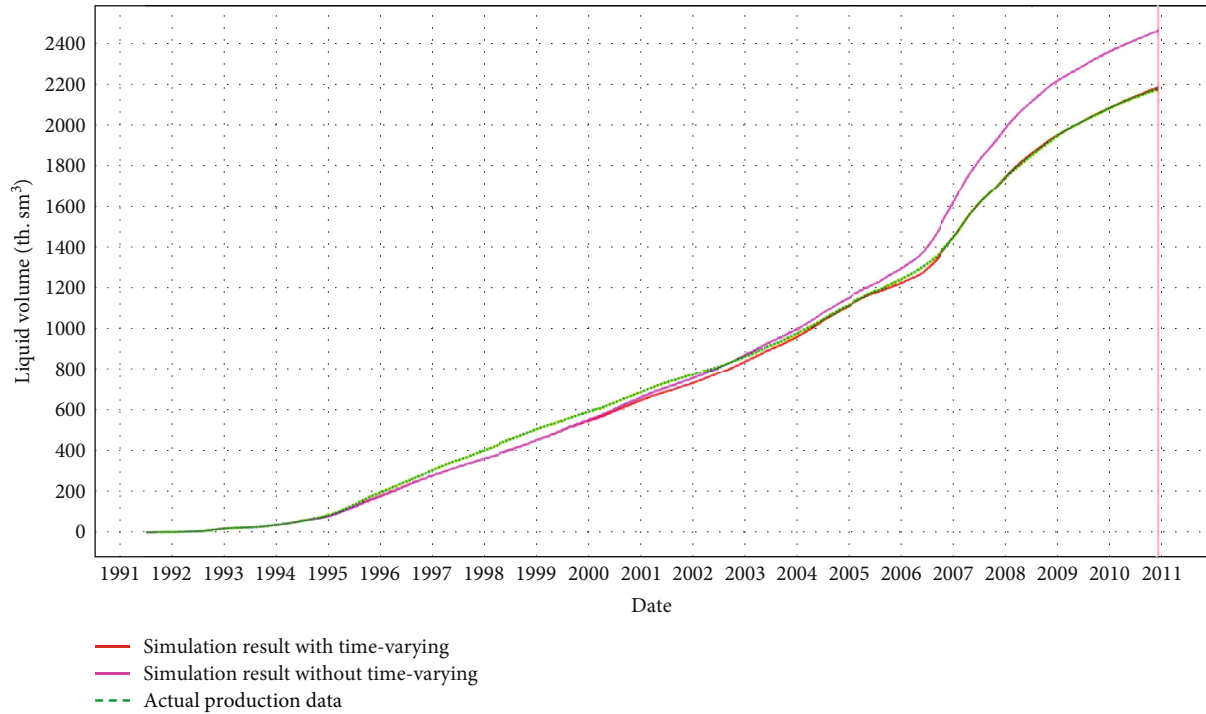
(a) Total oil production
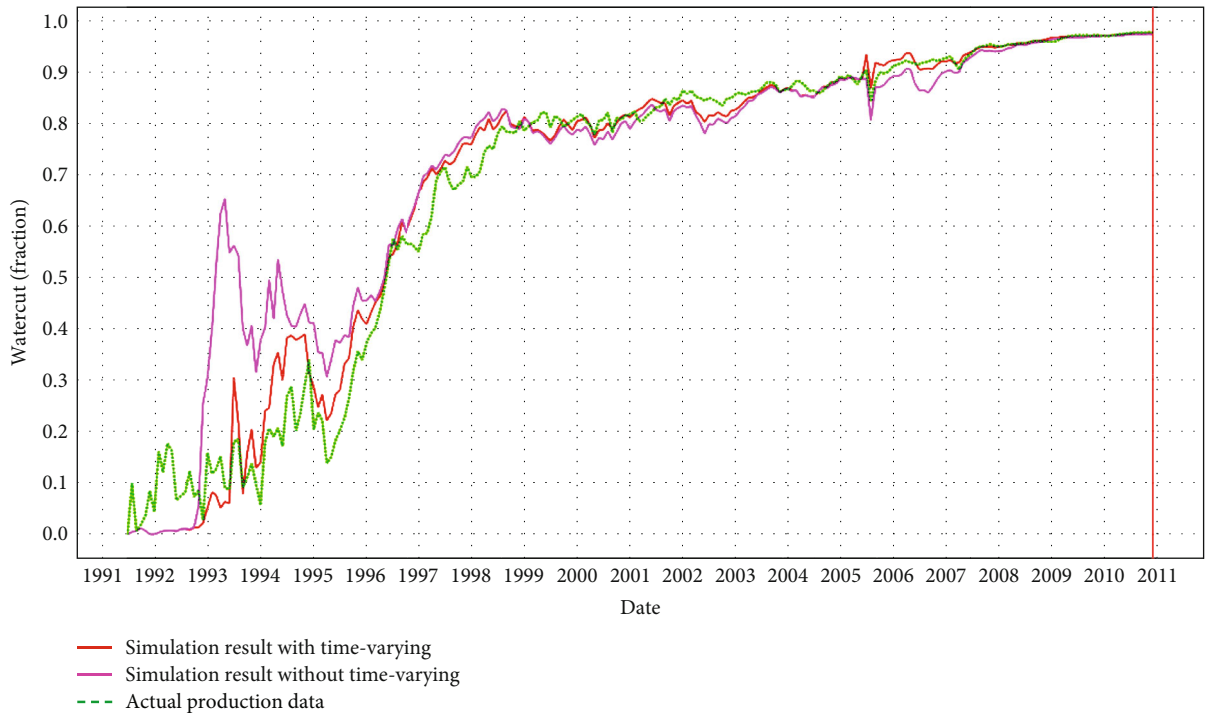
(b) Water cut

FIGURE 18: Result curve of total oil production and water cut.

is usually required to be controlled within an order of magnitude, and the logging interpretation is the well point value, the permeability calculated by the model represents the average value within 20 m around the well point. This value is affected by the surrounding grid and cannot fully represent the well-point value. Therefore, the accuracy of the results

is higher, indicating that the accuracy of the above method is better.

4.2. Comparison of Permeability before and after Water Flooding. The permeability model before and after water flooding is shown in Figure 15. Through the statistics of the

TABLE 10: Relative error between actual production data and simulation result.

Actual production data		Simulation result		Relative error (%)	
Total oil production ($10^4 \, m^3$)	Water cut (%)	Total oil production ($10^4 \, m^3$)	Water cut (%)	Total oil production ($10^4 \, m^3$)	Water cut (%)
217.4	97.7	218.3	97.3	-0.4	-0.4

permeability distribution range of different lithofacies after water flooding, as shown in Figure 16, it is found that for fine sandstone facies, the unimodal state before water flooding changes to the bimodal state after water flooding. The peak value changes from 300~1000 mD before water flooding, but the value changes obtained 300 mD and 1000~3000 mD after water flooding. Due to the influence of reservoir heterogeneity, the regional water injection with permeability less than 300 mD is difficult to spread, resulting in little change in the proportion. The proportion of permeability between 300 and 1000 mD decreases greatly, and the proportion of permeability greater than 1000 mD increases significantly, mainly due to the increase of permeability in the 300-1000 mD region.

For the middle sandstone facies, the proportion of permeability intervals before and after water flooding is bimodal, but it is obviously shifted to the high-permeability interval and gradually tends to an unimodal state greater than 5000 mD. The proportion of permeability lower than 300 mD also changes little, the proportion of 300~1000 and 1000~3000 mD decreases significantly, and the proportion greater than 5000 mD increases significantly. The main reason is that the permeability of 1000~3000 and 3000~5000 increases.

Numerical simulation cannot simulate changes in particle size, but it can simulate changes in porosity and permeability. As shown in Figure 17, the variation pattern of porosity before and after water flooding and the variation pattern of permeability in Figure 16 show that the porosity and permeability of fine sandstone and medium sandstone both increased.

The result of history match from Figure 18 and Table 10 shows that the result is much more accurate when considering the permeability variation; the relative error of total oil production and water cut is -0.4%.

5. Conclusions

(1) For high-permeability sandstone with high clay mineral content, the long-term water injection and the swelling of water-sensitive minerals made the mineral structure destroy, collapse, even dissolve and wash out by water, which further broadened the seepage channel and blocked some small holes

(2) Due to the high clay minerals in fine sandstone, erosion effects led to a significant increase in pore throats smaller than $5 \, \mu m$ and larger than $25 \, \mu m$. The heterogeneity including porosity and permeability was higher than those of medium sandstone

(3) Through the logging interpretation results of 4 development wells in the process of water flooding, the relative error of permeability less than 30% was much lower than the usual requirement of permeability error within one order of magnitude, which reflected the method was reasonable

(4) Comparing the permeability models before and after water flooding, the injected water in the area below 300 mD was difficult to spread, resulting in little change in permeability. The permeability in the areas of more than 300 mD and 1000~3000 mD increased obviously in the fine sandstone facies. The area of middle sandstone facies greater than 5000 mD increased mainly due to the increase of permeability in 1000~3000 mD interval and 3000~5000 mD interval

Data Availability

Data are available on request.

Conflicts of Interest

The authors declare that they have no known competing financial interests or personal relationships that could have appeared to affect the work reported in this paper.

Acknowledgments

References

[1] S. Mahmood, R. Masoud, and A. Shahab, "The impact of connate water saturation and salinity on oil recovery and CO_2 storage capacity during carbonated water injection in carbonate rock," *Chinese Journal of Chemical Engineering*, vol. 27, no. 7, pp. 1699–1707, 2019.

[2] R. K. Saw and A. Mandal, "Experimental investigation on fluid/fluid and rock/fluid interactions in enhanced oil recovery by low salinity water flooding for carbonate reservoirs," *Fuel*, vol. 352, article 129156, 2023.

[3] M. Akhlaghinia, F. Torabi, and C. W. Chan, "Effect of temperature on two-phase relative permeabilities of heavy oil, water, carbon dioxide, and methane determined by displacement technique," *Energy & Fuels*, vol. 27, no. 3, pp. 1185–1193, 2013.

[4] M. S. H. Bader, "Sulfate removal technologies for oil fields seawater injection operations," *Journal of Petroleum Science and Engineering*, vol. 55, no. 1-2, pp. 93–110, 2007.

[5] S. S. Behruz and S. Arne, "Enhanced oil recovery (EOR) by combined low salinity water/polymer flooding," *Energy & Fuels*, vol. 27, no. 3, pp. 1223–1235, 2013.

[6] N. Morrow and J. Buckley, "Improved oil recovery by low-salinity waterflooding," *Journal of petroleum Technology*, vol. 63, no. 5, pp. 106–112, 2011.

[7] S. O. Olayiwola and M. Dejam, "A comprehensive review on interaction of nanoparticles with low salinity water and surfactant for enhanced oil recovery in sandstone and carbonate reservoirs," *Fuel*, vol. 241, pp. 1045–1057, 2019.

[8] P. Rostami, F. Mohammad, M. F. Mehraban, M. Sharifi, M. Dejam, and S. Ayatollahi, "Effect of water salinity on oil/brine interfacial behaviour during low salinity waterflooding: a mechanistic study," *Petroleum*, vol. 5, no. 4, pp. 367–374, 2019.

[9] M. Vahid, K. Shahin, and D. Morteza, "EOR potential within Iran," *Special Topics Reviews in Porous Media: An International Journal*, vol. 5, no. 4, pp. 325–354, 2014.

[10] K. Sun, H. Liu, Y. Wang, L. Ge, and W. Du, "Novel method for inverted five-spot reservoir simulation at high water-cut stage based on time-varying relative permeability curves," *ACS Omega*, vol. 5, no. 22, pp. 13312–13323, 2020.

[11] R. J. Herz-Thyhsen, J. P. Kaszuba, and J. C. Dewey, "Dissolution of minerals and precipitation of an aluminosilicate phase during experimentally simulated hydraulic fracturing of a mudstone and a tight sandstone in the Powder River Basin, WY," *Energy & Fuels*, vol. 33, no. 5, pp. 3947–3956, 2019.

[12] S. Zhang, J. J. Sheng, and Z. Shen, "Effect of hydration on fractures and permeabilities in Mancos, Eagleford, Barnette and Marcellus shale cores under compressive stress conditions," *Journal of Petroleum Science and Engineering*, vol. 156, pp. 917–926, 2017.

[13] F. O. Ogunbanwo, W. Song, M. Steinsb, M. A. Fern, and A. R. Kovscek, "Mechanisms of multiphase reactive flow using biogenically calcite-functionalized micromodels," *Lab on a Chip*, vol. 18, no. 24, pp. 3881–3891, 2018.

[14] A. Ahmed and M. Ann, "Low salinity water injection: impact of physical diffusion, an aquifer and geological heterogeneity on slug size," *Journal of Petroleum Science and Engineering*, vol. 166, pp. 1055–1070, 2018.

[15] G. D. Cui, Y. Wang, Z. H. Rui, B. Chen, S. Ren, and L. Zhang, "Assessing the combined influence of fluid-rock interactions on reservoir properties and injectivity during CO_2 storage in saline aquifers," *Energy*, vol. 155, pp. 281–296, 2018.

[16] D. Arab, S. L. Bryant, O. Torsaeter, and A. Kantzas, "Water flooding of sandstone oil reservoirs: underlying mechanisms in imbibition vs. drainage displacement," *Journal of Petroleum Science and Engineering.*, vol. 213, article 110379, 2022.

[17] W. Q. Jin, X. J. Wang, F. P. He, and T. S. Chen, "Characteristics of Chang-6 oil-bearing formation changes after long term waterflood development in Ansai oilfield," *Journal of Earth Sciences and Environment*, vol. 32, pp. 239–244, 2010.

[18] L. O. Boampong, R. Rafati, and A. S. Haddad, "Evaluation of sour gas-low salinity waterflooding in carbonate reservoirs - a numerical simulation approach," *Journal of Petroleum Science and Engineering*, vol. 8, no. 2, pp. 131–150, 2023.

[19] N. Loahardjo, X. Xie, W. Winoto, J. S. Buckley, and N. R. Morrow, "Oil recovery by sequential waterflooding: the effect of aging at residual oil and initial water saturation," *Petroleum Exploration and Development*, vol. 39, no. 3, pp. 338–348, 2012.

[20] M. M. Marghani, M. Zairi, and A. E. Radwan, "Facies analysis, diagenesis, and petrophysical controls on the reservoir quality of the low porosity fluvial sandstone of the Nubian formation, east Sirt Basin, Libya: insights into the role of fractures in fluid migration, fluid flow, and enhancing the permeability of low porous reservoirs," *Marine and Petroleum Geology*, vol. 147, article 105986, 2023.

[21] M. A. Khan, T. Khan, A. Ali, A. M. Bello, and A. E. Radwan, "Role of depositional and diagenetic controls on reservoir quality of complex heterogenous tidal sandstone reservoirs: an example from the Lower Goru formation, Middle Indus Basin, Southwest Pakistan," *Marine and Petroleum Geology*, vol. 154, article 106337, 2023.

[22] Y. J. Ping, Z. S. Ren, L. B. Can, Z. G. Qiang, W. U. Jian, and L. D. Qiong, "Study on variation law of coalbed methane physical property parameters with seam depth," *International Journal of Coal Science & Technology*, vol. 42, no. 6, pp. 35–39, 2014.

[23] V. K. Sharma, A. Singh, and P. Tiwari, "An experimental study of pore-scale flow dynamics and heavy oil recovery using low saline water and chemical flooding," *Fuel*, vol. 334, article 126756, 2023.

[24] J. C. Xu, C. H. Guo, M. Z. Wei, and R. Z. Jiang, "Impact of parameters time variation on waterflooding reservoir performance," *Journal of Petroleum Science and Engineering*, vol. 126, pp. 181–189, 2015.

[25] P. I. Sagbana, K. Sarkodie, and W. A. Nkrumah, "A critical review of carbonate reservoir wettability modification during low salinity waterflooding," *Petroleum*, vol. 9, no. 3, pp. 2405–6561, 2023.

[26] R. Y. Cao, Z. H. Jia, L. S. Cheng, Z. Wang, T. Ye, and Z. Rui, "Using high-intensity water flooding relative permeability curve for predicting mature oilfield performance after long-term water flooding in order to realize sustainable development," *Journal of Petroleum Science and Engineering*, vol. 215, article 110629, 2022.

[27] N. Liu, B. S. Ju, Y. Yang, T. S. Brantson, J. Wang, and Y. P. Tian, "Experimental study of different factors on dynamic characteristics of dispersed bubbles rising motion behavior in a liquid-saturated porous media," *Journal of Petroleum Science and Engineering*, vol. 180, pp. 396–405, 2019.

[28] N. Liu, X. L. Chen, B. S. Ju et al., "Microbubbles generation by an orifice spraying method in a water-gas dispersion flooding system for enhanced oil recovery," *Journal of Petroleum Science and Engineering*, vol. 198, article 108196, 2021.